Cone-Beam X-ray Luminescence Computed Tomography Based on X-ray Absorption Dosage

Tianshuai Liu*, Junyan Rong*, Peng Gao, Wenlei Liu, and Hongbing Lu§
Department of Biomedical Engineering, Fourth Military Medical University, Xi'an, Shaanxi 710032, China
§*luhb@fmmu.edu.cn*

***Abstract*—Based on X-ray excitable particles, cone-beam X-ray luminescence computed tomography (CB-XLCT) has been proposed recently, which aims to achieve high-sensitivity optical imaging as well as high spatial resolution X-ray imaging. Currently, the imaging model of most XLCT systems is derived from the intensity distribution of X-ray within the object, not completely reflecting the nature of X-ray excitation process and X-ray scattering. To further improve the imaging quality of CB-XLCT, in this study, an imaging model based on X-ray absorption dosage is proposed. As the inverse problem is seriously ill-conditioned, an adaptive Tikhonov Regularization method is used for image reconstruction of CB-XLCT. Imaging experiments with numerical simulations and a physical phantom indicate that when compared with the model based on X-ray intensity, the proposed model based on X-ray dosage improves the image quality of CB-XLCT significantly.**

Keywords—X-ray dose; X-ray luminescence computed tomography;X-ray imaging; image reconstruction

I. INTRODUCTION

Based on X-ray excitable particles (nanophosphor particles), X-ray Luminescence Computed Tomography (XLCT) has been proposed recently as a new imaging modality [1-3]. Compared with traditional optical molecular imaging such as bioluminescence tomography (BLT) [4, 5] and fluorescence molecular tomography (FMT) [6, 7], XLCT can achieve high-sensitivity optical imaging as well as high spatial resolution X-ray imaging because of the use of X-ray. Because of the advantages of XLCT, it provides the possibility for clinical application, such as disease diagnosis, drug delivery and photodynamic therapy.

After XLCT was demonstrated for the first time [1], continuous studies have been devoted in XLCT imaging by many researchers. The narrow-beam [3] could achieve better spatial resolution and imaging depth but need long imaging time because of the complicated data acquisition model. To reduce the imaging time, a cone-beam XLCT (CB-XLCT) imaging system was investigated recently by Chen et al [8-10], and applied to small animal imaging by Liu et al [11]. Compared with narrow-beam XLCT, CB-XLCT could speed up imaging significantly. However, the imaging model of most XLCT systems is derived from the intensity distribution of X-ray within the object, which could not reflect the nature of X-ray excitation process and X-ray scattering completely. For the excitation principle of nanoparticles, the excitation of nanoparticles depends more on absorbing the energy of X-ray. Compared with the X-ray intensity, X-ray dose is more relevant with X-ray energy. Especially, when used for in-vivo studies, it is difficult to calculate X-ray intensities inside the target due to different attenuation coefficients of different tissues and the scattering of X-rays in biological tissues. Considering the complicated process of CB-XLCT imaging, an accurate forward model would benefit imaging quality greatly.

In this paper, we propose an imaging model based on X-ray radiation dosage to improve the forward model of CB-XLCT. To evaluate the performance of the proposed model, X-ray dosage inside the imaging object was first estimated by the widely-used GATE package. Then numerical simulations of targets positioned at different depths and phantom experiments were carried out. With the use of an adaptive Tikhonov Regularization method for image reconstruction, our results indicate that when compared with the model based on X-ray intensity, the proposed model based on X-ray dosage improves the image quality of CB-XLCT significantly.

II. THEORY

A. CB-XLCT Imaging System

Fig 1 gives a schematic diagram of the CB-XLCT system and the custom-made system used in this study. The system included a cone beam X-ray source, a rotation stage for the object to be imaged, a flat-panel X-ray detector for high-resolution CT imaging, and an electron-multiplying charge-coupled device (EMCCD) camera for optical imaging. The maximum voltage of the X-ray source (Oxford Instrument, U.K.) used in the system is 80kV, with the maximum power of 80W. An electronic gain EMCCD camera(CCD-iXon+DU897) coupled with a Nikon 50-mm f/1.8D lens was positioned at 90° towards the X-ray source-detector axis, which was used to collect the emitted light signals. The minimum cooling temperature of EMCCD camera is -80 degrees, which can effectively reduce the dark noise.

*Co-first authors.

This work is supported by the National Natural Science Foundation of China, under Grant No. 81230035

DOI: 10.12059/Fully3D.2017-11-3203003

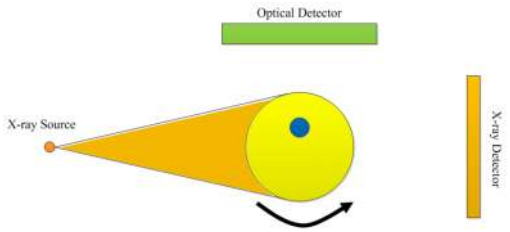

(a)

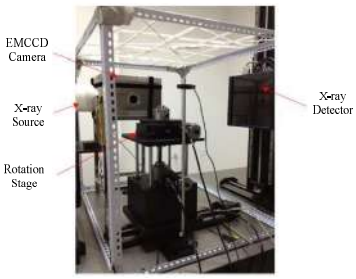

(b)

Fig. 1.The schematic diagram of the CB-XLCT system. (b) A photo of CB-XLCT imaging system used in this study.

B. Forward model of XLCT

In XLCT imaging, X-rays emitted by the X-ray source travel through the biological tissues and provide an excitation field in the imaging object. Currently, the excitation field model of most XLCT systems is derived from the intensity distribution of X-ray within the object, which can be given by the Lambert-Beer law.

$$\mathrm{X}(\mathrm{r}) = \mathrm{X}(\mathrm{r}_0)\exp[-\int_{r_0}^{r}\mu_t(\tau)d\tau] \tag{1}$$

where $\mathrm{X}(\mathrm{r}_0)$ is the intensity of X rays at the initial position of r_0, $\mu_\tau(\tau)$ is the X-ray attenuation coefficient.

However, the intensity distribution of X-ray given by the Lambert-Beer law doesn't consider the scattering of X-ray, which will have an effect on X-ray intensity. Besides, the excitation of nanoparticles depends more on absorbing the energy of X-ray considering the excitation principle of nanoparticles. Compared with the X-ray intensity, X-ray dose is more relevant with X-ray energy. Therefore, the excitation field model of most XLCT systems is derived from the dosage distribution of X-ray within the object in our study, which can be estimated by the widely-used GATE package.

Irradiated by X-rays, the nanophosphors in the object emit visible or NIR light. Based on previous studies, the number of optical photons emitted by nanophosphors is related to the absorbed dose of X rays and the concentration of nanophosphor [3, 12].

$$\mathrm{S}(\mathrm{r}) = \varepsilon X_d(\mathrm{r})\mathrm{n}(\mathrm{r}) \tag{2}$$

where S(r) is the light source energy density, n(r) is the concentration of nanophosphors, ε is the light yield and $X_d(\mathrm{r})$ is the absorbed dose of X-rays at position *r*.

In the visible and NIR spectral window, biological tissues have the characteristics of high scattering and low absorption. Therefore, the propagation model of the emitted light in biological tissues can be established by the diffusion equation (DE) [13]:

$$-\nabla\cdot\left[\mathrm{D}(\mathrm{r})\nabla\Phi(\mathrm{r})\right]+\mu_\mathrm{a}(\mathrm{r})\Phi(\mathrm{r}) = \mathrm{S}(\mathrm{r})\ \ (\mathrm{r}\in\Omega) \tag{3}$$

where Ω is the image domain, $\Phi(\mathrm{r})$ is the photon fluence, $\mu_\mathrm{a}(\mathrm{r})$ is the absorption coefficient, $\mathrm{D}(\mathrm{r})$ is the diffusion coefficient which can be calculated by $\mathrm{D}(\mathrm{r}) = 1/[3(\mu_s^{'}(\mathrm{r})+\mu_\mathrm{a}(\mathrm{r})]$, in which $\mu_s^{'}(\mathrm{r})$ is the reduced scattering coefficient.

In order to solve the diffusion equation (3), the Robin boundary conditions are needed [14], as shown below:

$$\Phi(\mathrm{r})+2\kappa\mathrm{D}(\mathrm{r})\left[\nu\nabla\Phi(\mathrm{r})\right] = 0\ \ (\mathrm{r}\in\partial\Omega) \tag{4}$$

where $\partial\Omega$ is the boundary of Ω, κ is the boundary mismatch parameter and ν is the outer normal vector on the boundary.

Based on the finite element method (FEM), we can discretize Eqs.(2) and (3) into a matrix form and the forward model of XLCT can be given by

$$\Phi = \mathrm{W}X \tag{5}$$

where Φ is the photon fluence vector measured by the optical detector, W is the weight matrix and $X = [x_1, x_2, \cdots, x_n] = [n(r_1), n(r_2), \cdots, n(r_n)]$ is the unknown nanophosphors concentration vector to be reconstructed.

In our study, the forward model of XLCT is established based on the dosage distribution of X-ray within the imaging object. Then, the number of emitted photons is calculated by the dosage of X-rays, rather than the intensity of X-rays. Compared with the forward model based on X-ray intensity, the proposed model based on X-ray dosage take the scattering of X rays into account and which is more suitable for the excitation principle of nanophosphors.

C. Image Reconstruction of CB-XLCT

Based on the forward model, the image reconstruction of CB-XLCT is the solving process of X from Φ .XLCT image reconstruction is an ill posed problem where the solution is usually underdetermined and noise sensitive. In this study, an adaptive Tikhonov regularization method (ADAPTIK) is used to solve the CB-XLCT inverse problem.

The solution of Tikhonov regularization (TR) to Eqs. (5) can be given by

$$X = [W^TW+\alpha I]W^T\Phi \tag{6}$$

It can be seen that in the TR method, all the pixels in the image are reconstructed by the same regularization parameter,

which cause that the distribution region of the fluorescent probe and get the same smoothness constraint with region of the background. When the larger α is used to obtain the high SNR image, the distribution region of the fluorescent probe is also excessively smooth, which lead to the low resolution of reconstruction. In order to improve the quality of the reconstruction, different regularization parameters are used to smooth constraints for different regions in Adaptik method [15].

$$X_n = [W^T W + \Lambda I]^{-1} W^T \Phi \tag{7}$$

where Λ is a diagonal matrix composed of spatially varying regularization parameters

$$\Lambda = \begin{Bmatrix} \alpha_n(r) & \cdots & 0 \\ \vdots & \ddots & \vdots \\ 0 & \cdots & \alpha_n(Nv) \end{Bmatrix} \tag{8}$$

where $\alpha_n(r)$ is regularization parameter which can be updated according to the results of the previous iteration.

$$\alpha_n(r) = \begin{cases} \alpha_{n-1}(r) & X_{n-1}(r) = 0 \\ \gamma\alpha_{n-1}(r) & X_{n-1}(r) > 0 \end{cases} \tag{9}$$

Where γ is the contraction factor which can be given by

$$\gamma = \sqrt[N]{\alpha_{stop}} \tag{10}$$

where N is iteration number, α_{stop} is the cutoff regularization parameter.

Based on this method, the unknown distribution of nanophosphors can be obtained consistently, where the area with fluorescent probe distribution is preserved and the background area is smoothed.

III. EXPERIMENTAL DESIGN

To evaluate the impact of the proposed forward model on CB-XLCT reconstruction, the X-ray dose distribution within the imaging object should be estimated first. In this study, the widely-used Monte Carlo software package GATE (Gate V7.1) was used to estimate the absorbed X-ray dose in the phantom [16]. Then numerical simulations of targets positioned at different depths and phantom experiments were carried out to evaluate the performance of the proposed model based on X-ray dosage for CB-XLCT imaging. For comparison, the traditional forward model based on X-ray intensity calculated from Eqs. (1) was also used to reconstruct the images.

A. X-Ray Dose Estimation using GATE

The imaging system and experimental conditions were simulated by GATE to estimate the absorbed X-ray dose of a given phantom. The voltage and current of X-ray tube were set as 70kv and 0.8 mA. The distance from the X-ray source to a phantom was set as 26.3cm, which was consistent with our experimental conditions.

In this study, a large cylinder (3.0cm in diameter, 4.0cm in height) containing a mixture of water and agar was employed as the phantom. Another small cylinder (4mm in diameter, 4mm in height) filled with GOS: Eu^{3+} (concentrations: 100mg/ml) was placed inside the phantom as the target. In order to obtain absorbed X-ray dose at different depths, the target was positioned at different depths, as shown in Table I, and was built in GATE, as shown in Fig 2. For a full scan of the phantom, a dose map was obtained every 15 degrees from 0° to 360° for every depth.

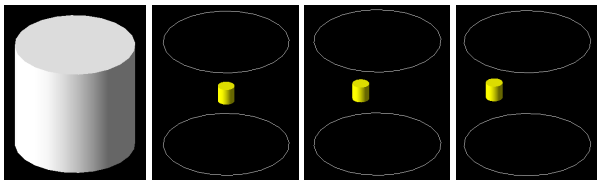

(a) **(b)** **(c)** **(d)**

Fig. 2.The phantom with the target positioned at different depths in Gate. (a) Phantom (b) 15mm, (c) 11mm, and (d) 7 mm.

TABLE I. DEPTH OF TARGET IN THE PHOTOM

Depth/mm	15	11	7

B. Numerical Simulations

Numerical Simulations with the target positioned at different depths were first implemented to test the performance of the proposed model for CB-XLCT. All the simulations were based on the forward model described in Eqs. (2)-(5). The X-ray dose was estimated by GATE and the light yield ε was set to be 0.15cm^3/mg [17].

Fig 3 gives the simulated phantom with the target positioned at different depths. The optical properties of the phantom were set as $\mu_a = 0.0072mm^{-1}$ and $\mu_s' = 0.72mm^{-1}$ at the wavelength of 703nm, which is the peak value in the emission spectrum of GOS:Eu^{3+} [18].

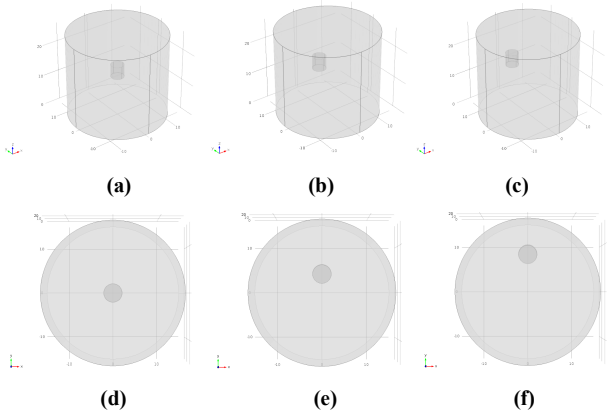

(a) **(b)** **(c)**

(d) **(e)** **(f)**

Fig 3.The simulation model for different depths. (a), (b), (c) the three dimensional diagram correspond to depth 15,11,7 mm, (d), (e), (f) the overhead view correspond to depth 15,11,7 mm

The simulated model was rotated from 0° to 360°and a projection image was obtained every 15 degrees. Zero-mean white Gaussian noise was added into the projections with a signal-to-noise ratio (SNR) of 35 DB. The ADAPTIK method was used to reconstruct nanoparticle distributions based on the X-ray dose model and the X-ray intensity model, respectively.

C. Phantom Experiments

Phantom experiments were conducted using the custom-made imaging system. A glass cylinder (3.0cm in diameter, 4.0cm in height) containing a mixture of water and agar was fixed on the rotation stage. A glass tube (4mm in diameter) filled with GOS: Eu^{3+} (with concentration of 100mg/ml) was placed into the cylinder, as shown in Fig 4. The voltage and current of the X-ray source were set to 70 KV and 0.8mA, respectively.

The phantom was rotated from 0° to 360°and a projection image was obtained every 15 degrees by the EMCCD camera. The exposure time of EMCCD camera was set as 2 s. Since the rotation speed of the phantom was 6°/s, the total time for a full rotation was 60 s. Therefore, the XLCT imaging time for 24 projections was about 108 s .

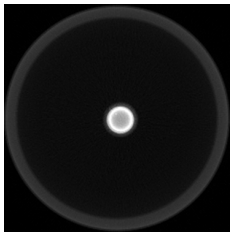

Fig.4.Representative X-ray CT(XCT) slice of the phantom

IV. RESULTS

A. X-Ray Dose Measurement

Fig.5 demonstrates the dose maps estimated by GATE. For each depth, dose maps obtained at 5 representative angles were compared.

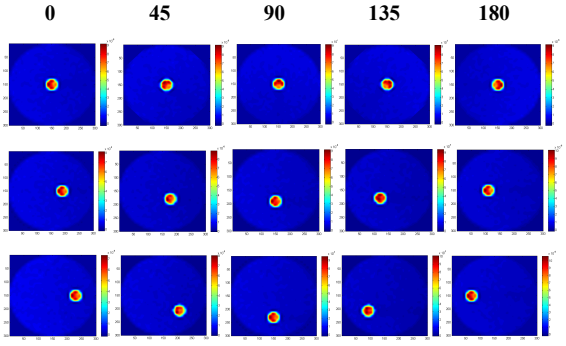

Fig.5.Dose map for different projections at different depths. Row 1-3 correspond to the depth of 15,11,7 mm, respectively.

B. Numerical Simulations

The reconstructed images of the numerical simulations are shown in Fig 6. Figs 6(a), (c), (e) illustrate the reconstructed slice and 3D rendering results using the proposed model for targets at three different depths. Figs 5(b), (d), (f) show the corresponding reconstruction results using the X-ray intensity model. It clearly indicates that at each depth, the proposed CB-XLCT model based on X-ray dosage yields better image quality in terms of target shape and localization accuracy than the X-ray intensity model.

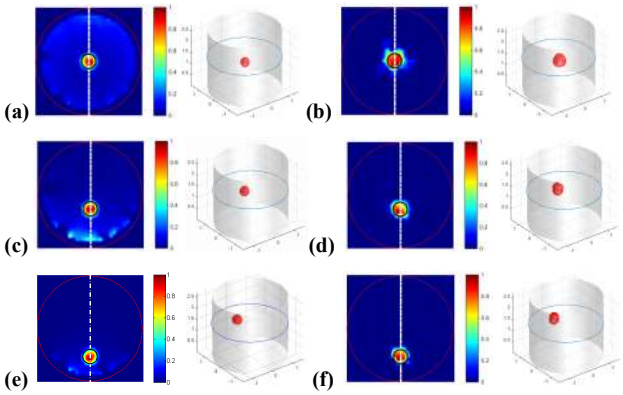

Fig.6.CB-XLCT reconstructions using the X-ray dose model (left) and the X-ray intensity model (right). (a), (b) For a target positioned at depth 15mm. (c), (d) For a target positioned at depth 11mm. (e), (f) For a target positioned at depth 7mm.

C. Phantom Experiments

The reconstruction image of the phantom experiments are shown in Fig 7. Fig 7(a) illustrates the reconstructed slice, Fig 7(b) presents the fusion of XLCT and XCT images and Fig 7(c) shows the 3-D rendering of the reconstruction results of CB-XLCT model based on X-ray dose. Fig 7(d), (e), (f) show the corresponding reconstruction results of CB-XLCT model based on X-ray intensity. In contrast, the proposed CB-XLCT model based on X-ray dosage achieves better image quality in terms of target shape and localization accuracy than the X-ray intensity model.

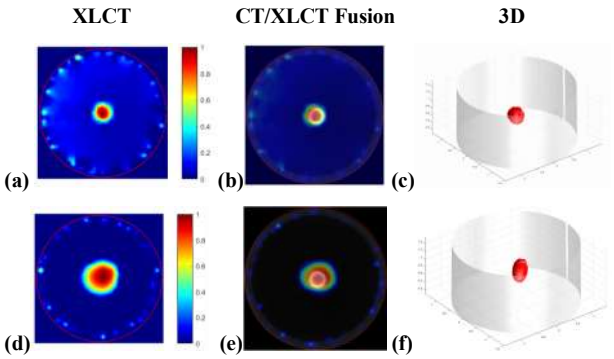

Fig 7.The reconstruction result of the phantom experiments. (a), (d) show the reconstruction results of CB-XLCT model based on X-ray dose and X-ray intensity. (b), (e) present the fusion of XLCT and XCT images. (c), (f) show the 3-D rendering of the XLCT reconstruction results.

V. CONSLUSIONS

Considering the scattering of X-ray, the X-ray intensity model calculated by the Lambert-Beer law is not consistent with the experimental condition perfectly. Besides, the excitation of nanoparticles depends more on absorbing the energy of X-ray considering the excitation principle of nanoparticles. Compared with the X-ray intensity, X-ray dose is more relevant with X-ray energy. In this work, we establish a forward model based on X-ray absorption dosage for CB-XLCT imaging. The reconstruction result of numerical simulations and phantom experiments indicate that the proposed model can improve the image quality of CB-XLCT

significantly, when compared with the model based on X-ray intensity. Considering the benefit of CB-XLCT for *in-vivo* studies, our future work will focus on how to estimate X-ray absorption dose in a complex phantom and *in-vivo* experiments accurately.

REFERENCES.

[1] G. Pratx, C. M. Carpenter, C. Sun, and L. Xing, "X-ray luminescence computed tomography via selective excitation: A feasibility study," IEEE Trans. Med. Imag., vol. 29, no. 12, pp. 1992–1999, 2010.

[2] G. Pratx, C. M. Carpenter, C. Sun, R. P. Rao, and L. Xing, "Tomographic molecular imaging of X-ray-excitable nanoparticles," Opt. Lett., vol. 35, no. 20, pp. 3345–3347, 2010.

[3] C. M. Carpenter, G. Pratx, C. Sun, and L. Xing, "Hybrid X-ray/optical luminescence imaging: Characterization of experimental conditions," Med. Phys., vol. 37, no. 8, pp. 4011–4018, 2010.

[4] G. Wang, W. Cong, K. Durairaj, X. Qian, H. Shen, P. Sinn, E. Hoffman, G. McLennan, and M. Henry, "In vivo mouse studies with bioluminescence tomography," Opt. Express, vol. 14, no. 17, pp. 7801–7809, 2006.

[5] J. Feng, C. Qin, K. Jia, S. Zhu, X. Yang, and J. Tian, "Bioluminescence tomography imaging in vivo: Recent advances," IEEE J. Sel. Top. Quant., vol. 18, no. 4, pp. 1394–1402, 2012.

[6] A. Ale, V. Ermolayev, E. Herzog, C. Cohrs, M. H. de Angelis, and V. Ntziachristos, "FMT-XCT: in vivo animal studies with hybrid fluorescence molecular tomography-X-ray computed tomography," Nat. Methods, vol. 9, pp. 615–620, 2012.

[7] G. Zhang, F. Liu, B. Zhang, Y. He, J. Luo, and J. Bai, "Imaging of pharmacokinetic rates of indocyanine green in mouse liver with a hybrid fluorescence molecular tomography/x-ray computed tomography system," J. Biomed. Opt., vol. 18, no. 4, pp. 040505-1–040505-3, 2013.

[8] D. Chen, S. Zhu, H. Yi, X. Zhang, D. Chen, J. Liang, and J. Tian, "Cone beam X-ray luminescence computed tomography: A feasibility study," Med. Phys., vol. 40, no. 3, pp. 031111-1–031111-14, 2013.

[9] D. Chen, S. Zhu, X. Chen, T. Chao, X. Cao, F. Zhao, L. Huang, and J. Liang, "Quantitative cone beam X-ray luminescence tomography-X-ray computed tomography imaging," Appl. Phys. Lett., vol, 105, no. 19, pp. 191104-1–191104-4, 2014.

[10] D. Chen, S. Zhu, X. Cao, F. Zhao, and J. Liang, "X-ray luminescence computed tomography imaging based on X-ray distribution model and adaptively split Bregman method," Biomed. Opt. Express, vol. 6, no. 7, pp. 2649–2663, 2015.

[11] X. Liu, Q. Liao and H. Wang, In vivo x-ray luminescence tomographic imaging with single-view data, OPT LETT, vol. 38, (no. 22), pp. 4530-4533, 2013.

[12] Li C, Martínez-Dávalos A, Cherry S R. Numerical simulation of x-ray luminescence optical tomography for small-animal imaging.[J]. Journal of Biomedical Optics, 2014, 19(4):523-9.

[13] Zhang G, et al. Cone Beam X-ray Luminescence Computed Tomography Based on Bayesian Method.[J]. IEEE Transactions on Medical Imaging, 2016.

[14] X. Liu, Q. Liao and H. Wang, Fast X-Ray Luminescence Computed Tomography Imaging, Biomedical Engineering, IEEE Transactions on, vol. 61, (no. 6), pp. 1621-1627, 2014-01-01 2014.

[15] Cao X, Zhang B, Wang X, et al. An adaptive Tikhonov regularization method for fluorescence molecular tomography[J]. Medical & Biological Engineering & Computing, 2013, 51(8):849-58.

[16] A. Mittone, F. Baldacci, A. Bravin, E. Brun, F. Delaire, C. Ferrero, S. Gasilov, N. Freud, J. M. Létang, D. Sarrut, et al., "An efficient numerical tool for dose deposition prediction applied to synchrotron medical imaging and radiation therapy.", Journal of synchrotron radiation, vol. 20, issue Pt 5, pp. 785-92, 2013.

[17] W. Cong, H. Shen, and G. Wang, "Spectrally resolving and scattering compensated X-ray luminescence/fluorescence computed tomography," J. Biomed. Opt., vol. 16, no.6, pp. 066014-1–066014-7, 2011.

[18] Zhang W, Zhu D, Lun M, et al. Multiple pinhole collimator based X-ray luminescence computed tomography.[J]. Biomedical Optics Express, 2016, 7(7).